RSC Advances

PAPER

View Article Online
View Journal | View Issue

Cite this: *RSC Adv.*, 2025, **15**, 12713

Dual-drive mica-based magnetic composite phase-change materials for photothermal and magnetothermal conversion

Xiaofei Li,[a] Yinao Jiao,[b] Yupeng Li,[a] Cheng Pan, *[b] Guozhi Fan,[b] Yifei Long,[b] Qunpeng Cheng[b] and Haitao Yang *[a]

Received 25th September 2024
Accepted 21st February 2025

DOI: 10.1039/d4ra06902a

rsc.li/rsc-advances

To extend the applications of phase-change materials to multiple scenarios, Fe_3O_4 nanoparticles were deposited on the surface of mica with a layer-like structure using a simple method, and composite phase-change materials (CPCMs) with dual-driven energy conversion performance were subsequently obtained *via* vacuum impregnation. The addition of boron nitride (BN) and cellulose nanofibers (CNFs) endowed the CPCMs with higher thermal conductivity (0.85 W m^{-1} K^{-1}) and lower specific heat capacity (1.42 MJ m^{-2} K^{-1}), thereby constructing an effective heat transfer channel. The photothermal conversion efficiency of the CPCMs reached up to 88.36%. The magnetic Fe_3O_4 nanoparticles endowed the CPCMs with magnetic responsiveness, enabling the phase transition process to complete within just 112 s under a magnetic field. With a high phase-change material loading (82.65%), the CPCMs maintained excellent thermal stability during the energy conversion process. These results provide guidance for the preparation of CPCMs with multiple types of efficient energy conversion.

1. Introduction

With the depletion of fossil fuels and increasing atmospheric pollution, new energy sources are gradually entering the public's field of vision while also continuously promoting the development and progress of energy storage technologies.[1,2] In recent years, thermal energy storage (TES) has achieved large-scale market applications both economically and technologically, and it is also one of the important methods for energy storage.[3] TES has been widely applied in areas, such as energy-saving buildings,[4] industrial waste heat utilization,[5] and medical supplies.[6] The key challenge in advancing heat storage technology lies in the selection of suitable materials.[7,8] Phase-change materials (PCMs), such as paraffin,[9] polyethylene glycol (PEG),[10] and hydrated salts, have received increasing attention due to their high latent heat capacity, high energy density, and low cost.[11] However, there are still some problems to be solved in the practical application of phase-change materials. The primary issue is the leakage during the solid–liquid phase transition process; therefore, carrier materials are introduced to encapsulate and stabilize the PCMs.

A simple solution is to load the PCM into an effective carrier, such as expanded graphite (EG),[12] kaolin, or zeolite,[13] which can effectively prevent leakage during the phase-change process and also provide reliable support for the PCM during the conversion process. Natural mineral-based materials are often used as support materials for PCMs due to their diverse forms, stable structure, good thermal stability, easy availability, and cost-effectiveness.[14,15] Mica is a layered silicate mineral that possesses high insulation properties, chemical stability, and a unique sheet-like structure as a natural mineral-based material.[16] However, the introduction of a carrier material can lead to a decrease in the thermal properties of the entire composite phase-change material, such as thermal conductivity and thermal energy storage enthalpy.

To improve the thermal energy storage performance of composite phase-change materials, the addition of functional fillers is particularly important.[17,18] For solar energy-absorbing materials, the optical and thermal properties of the fillers must be carefully considered to achieve effective photothermal energy conversion. Fe_3O_4 magnetic particles, with excellent light-absorbing properties and efficient magnetic response, were uniformly attached to the surface of mica carriers to solve the nanoparticle agglomeration problem and produce thermally conductive CPCMs with magneto-thermal conversion properties.[19] In addition to the light-absorbing and magneto-thermal conversion capabilities, the addition of functional fillers has had a positive impact on the energy conversion efficiency of CPCMs.[20–22] During photothermal or magnetothermal conversion, the converted thermal energy is transferred within the CPCMs along the thermal conduction path. The synergistic effect of functional fillers can effectively improve thermal conductivity and enhance energy conversion efficiency.[23–25] To

[a]*Hubei Provincial Key Laboratory of Green Materials for Light Industry, Hubei University of Technology, Wuhan, 430068, China*
[b]*School of Chemical and Environmental Engineering, Wuhan Polytechnic University, Wuhan, 430023, China. E-mail: ch_pan1018@whpu.edu.cn*

realize the uniform distribution of magnetic particles, three-dimensional magnetic heat-conducting structural materials are constructed through the directional arrangement of carriers.

Herein, we proposed a simple chemical deposition strategy to design CPCMs that integrated multifunctional photothermal and magnetothermal conversion and storage. Orientationally aligned mica-based composite phase-change materials were prepared by depositing magnetic Fe_3O_4 on the surface of mica carriers, followed by the vacuum impregnation method. The synergistic effect of functional fillers, such as BN and CNF, affected the thermal conductivity and heat transfer efficiency of CPCMs. In addition, the introduction of magnetic particles endowed the composite materials with magneto-thermal conversion performance. The dual-drive energy conversion efficiency of CPCMs was further studied, and the conversion mechanism was clarified, providing insights for the rational design and functional optimization of multi-drive composite materials.

2. Experimental

2.1 Materials

Oxalic acid (OA, 99.5% purity), ferric chloride hexahydrate, boron nitride (BN), and paraffin (PA) were supplied by Sinopharm Chemical Reagent Co., Ltd. (Shanghai, China). Cellulose nanofibers (CNFs) with a carboxyl content of 0.07% were obtained from Aladdin (Shanghai, China).

2.2 Preparation of mica-Fe_3O_4/CNF

To solve the problem of metal oxide particle agglomeration, the particles were anchored onto the surface of flake mica using a precise chemical hydrolysis method, resulting in the formation of mica-Fe_3O_4.

According to previous studies,[26] and as shown in Fig. 1, 1 g of mica and 3 g of OA were added to 3 g of a CNF aqueous solution (2% w/w) and stirred for 5 h at 90 °C. The resulting mixture was then washed and dried at 80 °C for 48 h, and the final product was labelled as mica-Fe_3O_4/CNF.

2.3 Preparation of CPCMs

The well-mixed solid powder (mica-Fe_3O_4/CNF and BN) was added to melted paraffin wax, stirred at 80 °C for 1 h, and then placed under vacuum for maceration to achieve adequate mixing. Subsequently, the mixture was quickly poured into a mold to form stable cylindrical CPCMs, labelled as mica-Fe_3O_4/CNF/BN/PA.

Furthermore, CPCMs were prepared by the same method using unmodified mica and CNF-modified mica as carriers and were labelled as mica/PA, mica/BN/PA, and mica/CNF/BN/PA.

2.4 Characterization

Scanning electron microscopy (SEM) and Fourier transform infrared spectroscopy (FT-IR) were used to analyze the microstructure and chemical structure of the CPCMs. X-ray diffraction (XRD) was used to determine their crystal structures. A thermogravimetric simultaneous thermal analyzer (TA) was used to evaluate the thermal and shape stability of the CPCMs under a nitrogen atmosphere from room temperature to 600 °C. The thermal properties of the CPCMs were evaluated by differential scanning calorimetry (DSC) under a nitrogen atmosphere from room temperature to 110 °C, with a heating/cooling rate of 5 °C min^{-1}. The thermal conductivity, specific heat capacity, and thermal diffusion coefficient of the CPCMs were measured using a transient planar heat source thermal conductivity meter. The temperature changes of the CPCMs during heating/cooling were recorded using an infrared thermal imaging instrument. An optical/magnetic-thermal conversion simulation device, consisting of a computer, xenon lamp light source or magnetic field generator, K-type thermocouple, and data acquisition system, was used to measure the photothermal and magnetothermal conversion performance of the CPCMs.

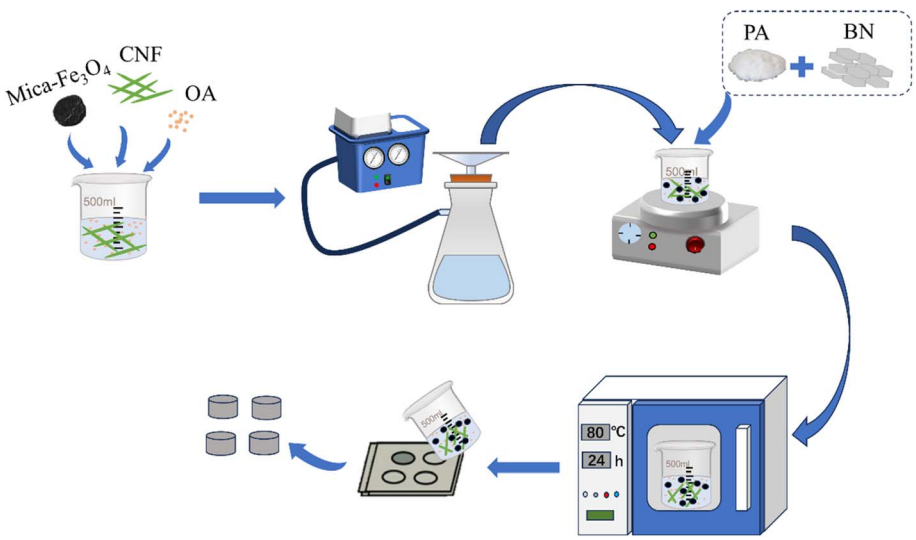

Fig. 1 Schematic of the preparation procedure for mica-Fe_3O_4/CNF/BN/PA.

3. Results and discussion

3.1 Morphology and crystal structure of CPCMs

The functional groups in the CPCMs—mica/PA, mica/BN/PA, mica/CNF/BN/PA, and mica-Fe_3O_4/CNF/BN/PA—were analyzed using FT-IR spectroscopy, as shown in Fig. 2a. The characteristic peaks at 3430 cm^{-1} and 1590 cm^{-1} corresponded to the symmetric stretching vibration and bending vibration of the –OH group, respectively. The intensity of the absorption peak at 3430 cm^{-1} in mica-Fe_3O_4/CNF/BN/PA reduced ignificantly, primarily due to the replacement of –OH groups on the mica surface by Fe^{3+}. Two strong absorption peaks at 2920 cm^{-1} and 2850 cm^{-1} were attributed to $-CH_2$ and $-CH_3$ groups in the material introduced by PA and CNF,[27] corresponding to C–H telescoping vibration. Additionally, two characteristic peaks at 814 cm^{-1} and 723 cm^{-1} indicated the formation of hydrogen bonds between mica and CNF during the recombination process. By comparing the infrared spectra of several sets of composite phase-change materials, no additional peaks were observed, indicating that no new substances were produced during the process. Meanwhile, XPS spectral analysis (Fig. 2c) clearly showed that the peaks at 288 eV, 530 eV, and 733 eV corresponded to the elements C, O and Fe, respectively.

In addition, the crystal structure of the CPCMs was analyzed using XRD. As shown in Fig. 2b, due to the addition of PA in CPCMs, two intense diffraction peaks at 21.8° and 23.8° can be clearly seen, with no shift observed. This indicated that PA achieved stability in the CPCMs through simple physical mixing.[28] Strong diffraction peaks of mica were observed at 26.7° and 45.4°.[29] Meanwhile, the characteristic peak of Fe_3O_4 was observed in mica-Fe_3O_4/CNF/BN/PA at 30.1°.[30]

The planar and cross-sectional images of the CPCMs were observed using a scanning electron microscope (SEM), as shown in Fig. 3. The CPCMs exhibited a clear hierarchical three-dimensional stacked spatial structure, with many pores and cracks on the surface of the mica, which was loaded with a large amount of PA. The structure and morphology were stable and effectively prevented the leakage of the PCM. The results confirmed that the PCM had been successfully loaded onto the mica surface.

3.2 Thermal management behaviors of CPCMs

Thermal stability is an important index for the working range and application scenarios of CPCMs.[31,32] As shown in the TG curves (Fig. 4a), the PCM loadings of mica/PA, mica/BN/PA, mica/CNF/BN/PA, and mica-Fe_3O_4/CNF/BN/PA were 58.25%, 65.53%, 62.84%, and 82.65%, respectively. From the DTG curve (Fig. 4b), it can be seen that the maximum loss rates of mica/PA, mica/BN/PA, mica/CNF/BN/PA, and mica-Fe_3O_4/CNF/BN/PA

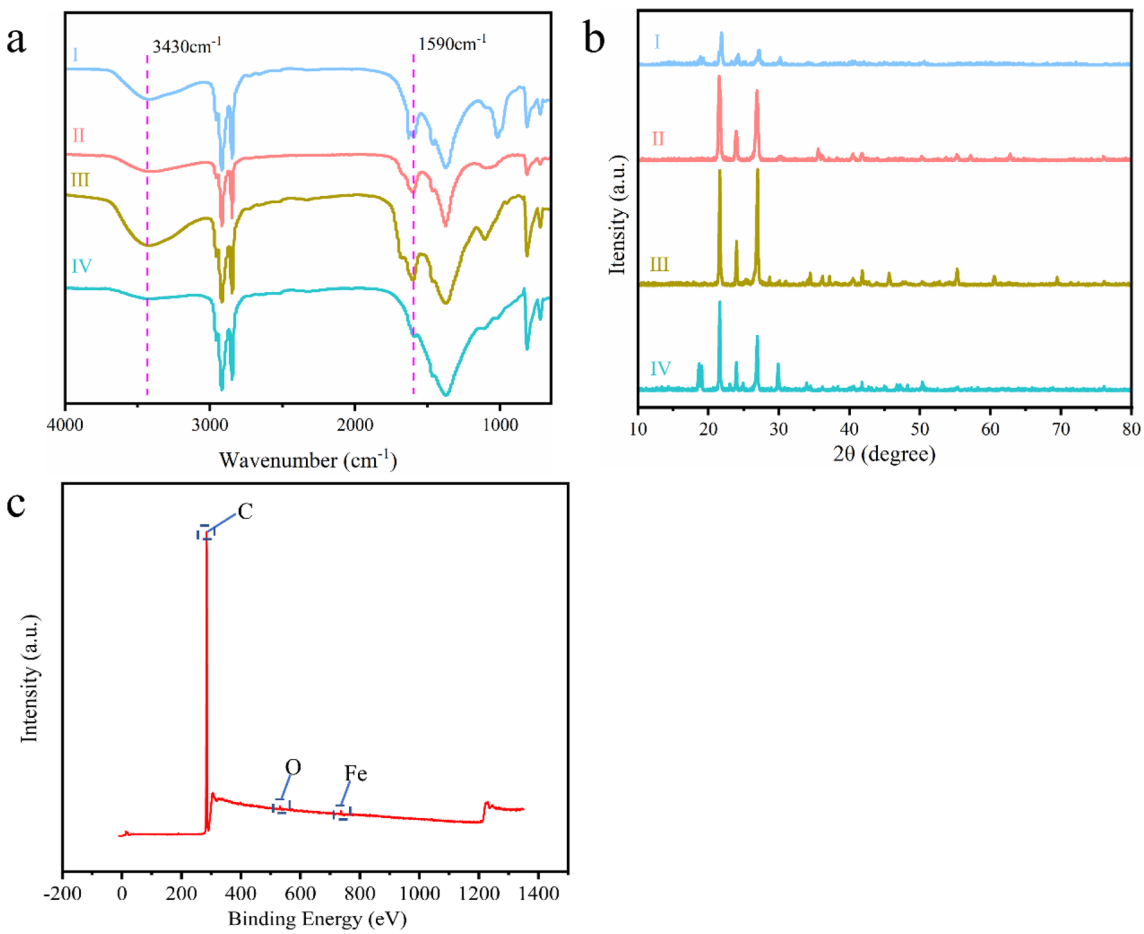

Fig. 2 FT-IR, (a) XRD, (b) and XPS (c) analysis of CPCMs (I: mica/PA, II: mica/BN/PA, III: mica/CNF/BN/PA, IV: mica-Fe_3O_4/CNF/BN/PA).

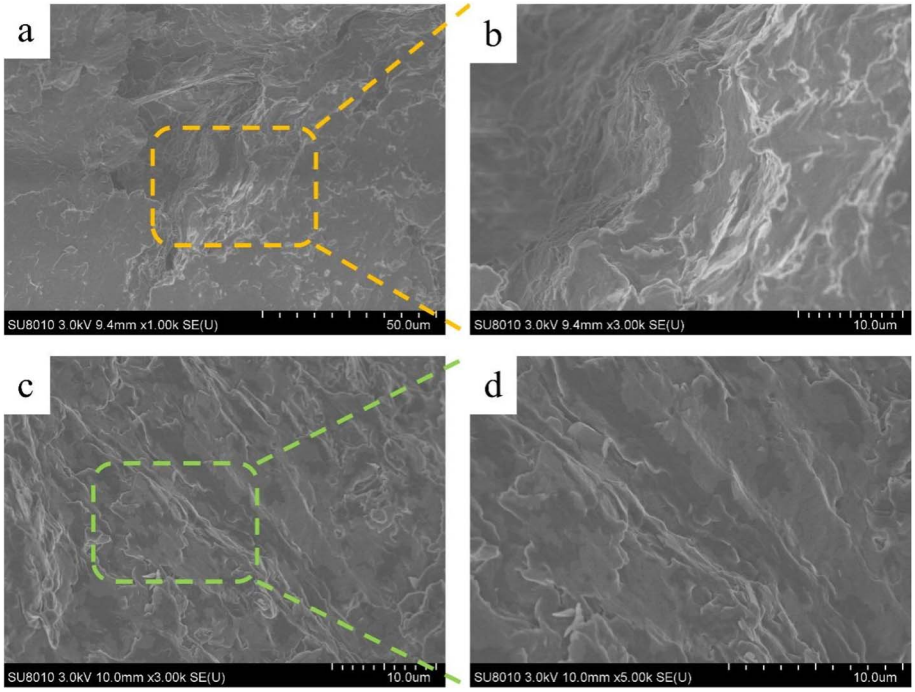

Fig. 3 Top views (a and b) and cross-sectional images (c and d) of CPCMs.

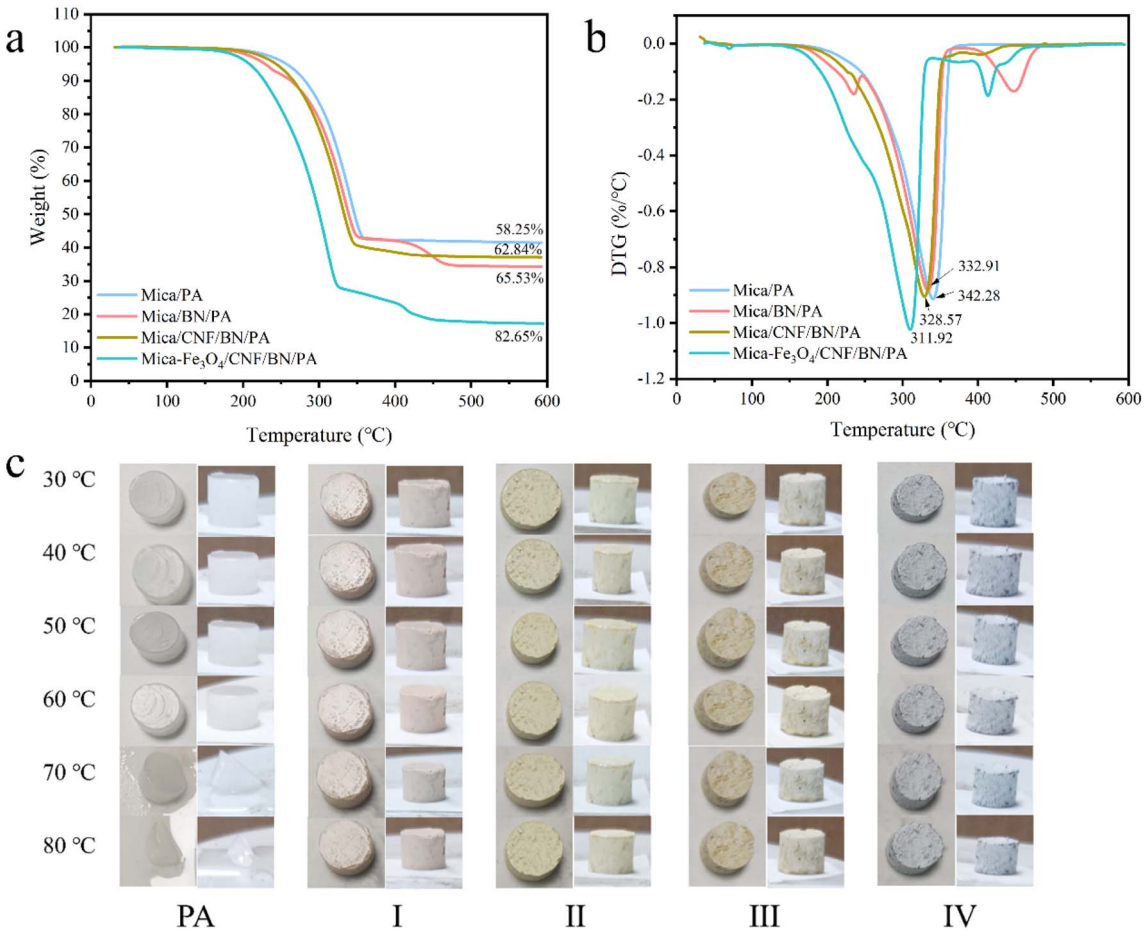

Fig. 4 TG (a), DTG (b), and stability testing (c) of CPCMs.

were 0.91%/°C at 342.28 °C, 0.87%/°C at 332.91 °C, 0.90%/°C at 328.57 °C, and 1.02%/°C at 311.92 °C, respectively. These losses mainly originated from the thermal decomposition of PA. The phase transition temperature of the CPCMs ranged between 50 °C and 70 °C, and the temperature during the energy conversion process did not exceed 100 °C. The working conditions of the composite phase-change material will not exceed the pyrolysis temperature of the phase-change material (around 300 °C).

In addition, the prepared cylindrical material was heated to visually verify that the CPCM maintained a relatively stable morphology even at low to medium temperatures. As shown in Fig. 4c, paraffin was used as a blank control, and the top and side views of the samples were taken. During the heating process, pure paraffin began to melt at 70 °C and was almost completely melted at 80 °C. In contrast, no obvious PCM leakage was observed in case of the prepared CPCMs throughout entire testing process, which indicated that the mica-based composites had reliable thermal stability in different temperature environments.

DSC analysis was used to investigate the thermal energy storage properties of the CPCMs. Fig. 5a and b shows the DSC curves of mica/PA, mica/BN/PA, mica/CNF/BN/PA, and mica-Fe_3O_4/CNF/BN/PA. No new peaks were observed, except for the displacement of the melting and crystallization peaks that appeared during the phase transition. These results indicated that the addition of fillers, such as CNF and BN, did not alter the chemical structure of the CPCMs. Meanwhile, the heat storage capacity of the materials was visually evaluated by observing the latent heat of CPCMs. As observed in Fig. 5c and d, it was found that mica-Fe_3O_4/CNF/BN/PA possessed the highest latent heat of melting (ΔH_f) (96.86 J g^{-1}) and crystallization (ΔH_c) (101.60 J g^{-1}). CNF, BN, and Fe_3O_4 had a synergistic effect during the absorption and release of energy, which together improved the heat storage capacity of the CPCMs.

Thermal reliability, which was closely related to the long-term use of the material, was characterized by 50 DSC thermal cycling tests. As shown in Fig. 5e and f, the melting and crystallization peaks of the four CPCMs only shifted left and right, with no new peaks appearing. The results confirmed the

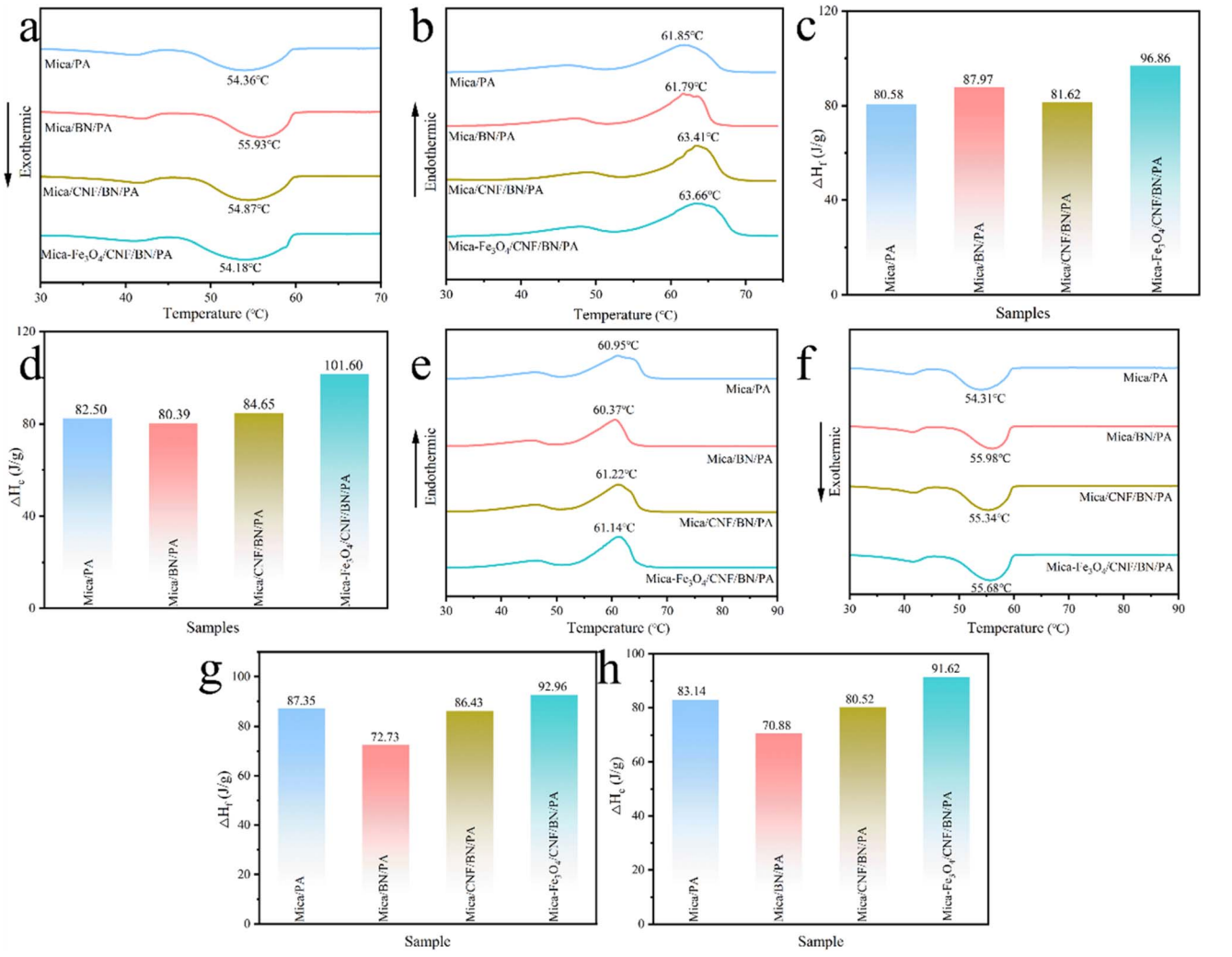

Fig. 5 (a) and (b) DSC of CPCMs, (c) melting enthalpy, (d) crystallization enthalpy, (e) and (f) DSC of CPCMs after 50 thermal cycling tests, (g) and (h) melting and crystallization enthalpy after 50 thermal cycling tests.

chemical stability of the materials over 50 thermal cycles. In addition, the latent heat of melting and crystallization of the CPCMs did not show a significant decrease and remained within a reasonable range of variation. This further proves that CPCMs have broad application potential in energy-saving buildings and industrial waste heat utilization.

The energy storage and release ability of the CPCMs are affected by thermal conductivity.[33] Compared to mica/PA (0.64 W m^{-1} K^{-1}), the thermal conductivity of mica/BN/PA (0.98 W m^{-1} K^{-1}), mica/CNF/BN/PA (0.91 W m^{-1} K^{-1}), and mica-Fe_3O_4/CNF/BN/PA (0.85 W m^{-1} K^{-1}) was enhanced by 53.13%, 42.19%, and 32.81%, respectively (Fig. 6a). In contrast, a high loading of PA decreased the thermal conductivity of mica-Fe_3O_4/CNF/BN/PA. The results indicated that the addition of CNF, BN, and Fe_3O_4 enhanced the thermal conductivity of the CPCMs. The heat diffusion coefficient of the CPCMs was inversely proportional to their specific heat capacity. Among them, the heat diffusion coefficient of mica/CNF/BN/PA was the largest (Fig. 6b). The phase transition behavior of the CPCMs was related to their specific heat capacity, which was also an important parameter affecting heat storage. The specific heat capacity of mica/PA was the highest, being 2.4 times greater than that of mica/CNF/BN/PA and mica-Fe_3O_4/CNF/BN/PA (Fig. 6c). The incorporation of CNF made the crystal structure of the CPCMs more orderly, thereby reducing their specific heat capacity. The addition of functional materials also led to a decrease in the latent heat capacity of the CPCMs. Through TG and DSC analysis, it was found that the Fe_3O_4-modified mica carrier was loaded with more phase-change materials, which resulted in an increase in the latent heat energy of the CPCMs. This, in turn, led to a relative decrease in thermal conductivity, though it remained much higher than that of the pure phase-change material. At the same time, the introduction of CNF and BN provided CPCMs with a good heat transfer channel, positively contributing to heat transfer during the energy conversion process.

Infrared thermography was used to demonstrate the heat absorption, exothermic, and temperature change processes of the CPCMs, with pure paraffin used as a comparison reference. As shown in Fig. 6d, the color of mica-Fe_3O_4/CNF/BN/PA changed to red more quickly compared to mica/PA. This was mainly attributed to the high thermal conductivity of BN, Fe_3O_4, and CNF, along with their synergistic effect. In addition, during the cooling process, the time–temperature curve (Fig. 6e)

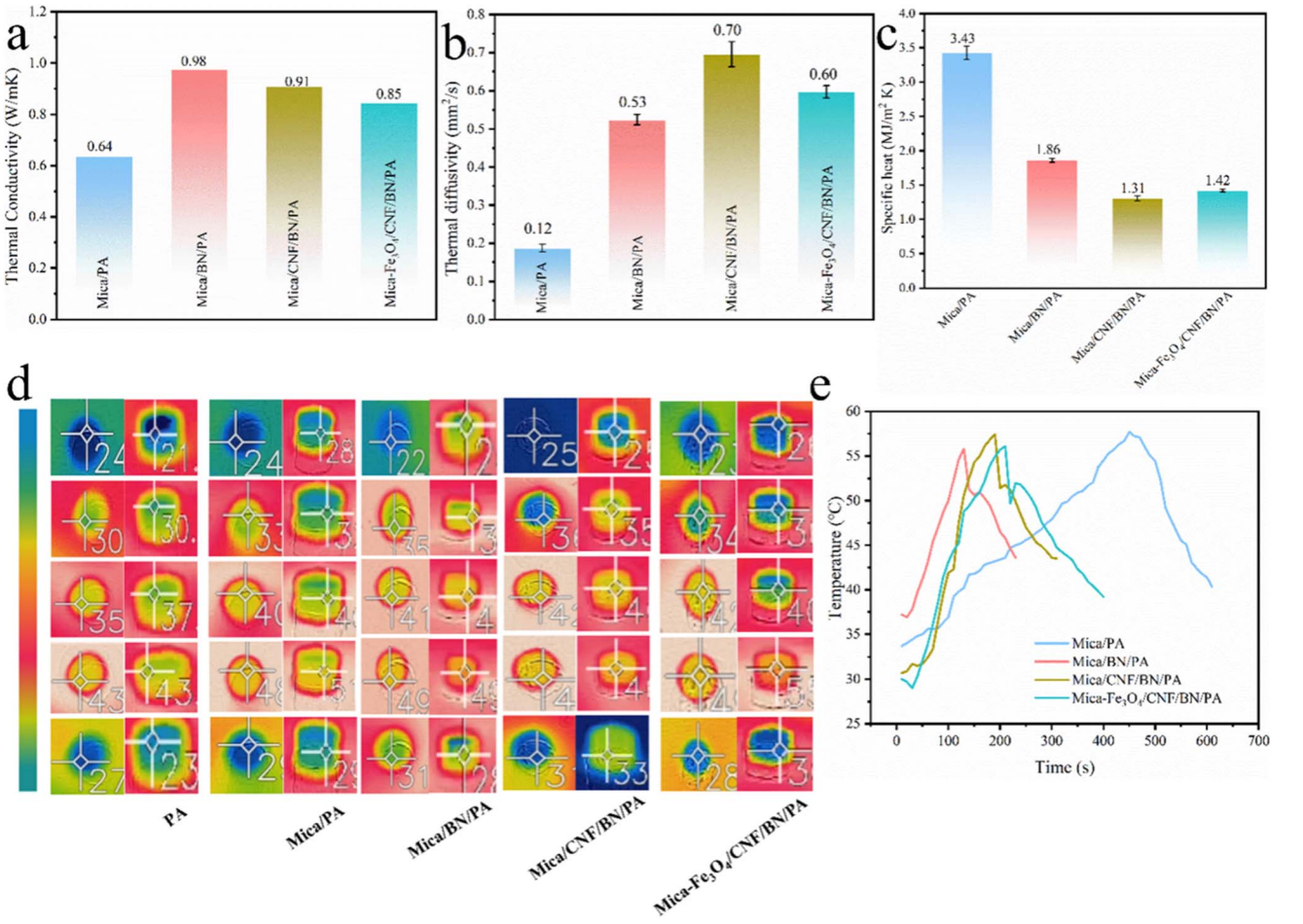

Fig. 6 The thermal conductivity (a), thermal diffusivity (b), specific heat capacity (c), infrared thermal imaging (d), and time–temperature curves (e) of CPCMs.

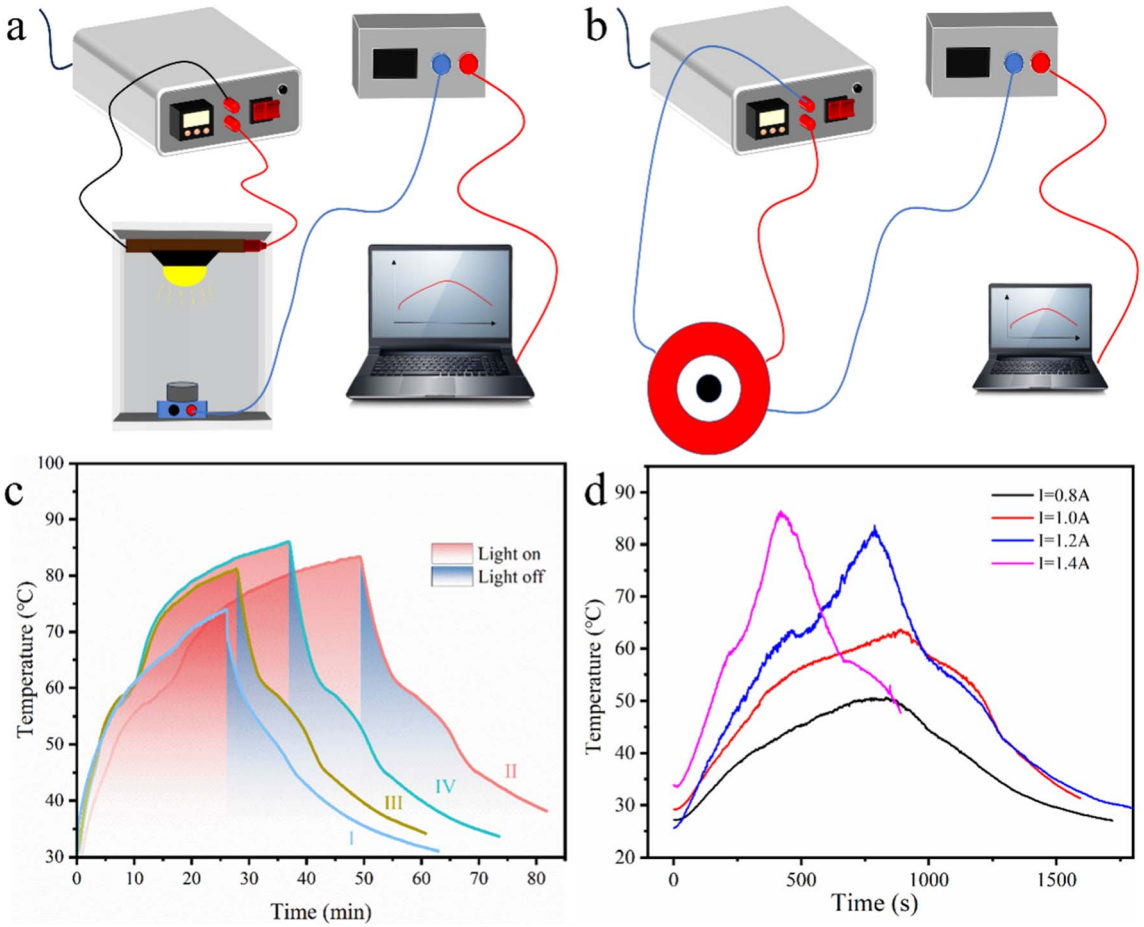

Fig. 7 Schematic of the experiments for photothermal conversion (a), magnetothermal conversion (b), thermal curve (c) of CPCMs (I: mica/PA, II: mica/BN/PA, III: mica/CNF/BN/PA, IV: mica-Fe_3O_4/CNF/BN/PA), and magnetic curve (d) of mica-Fe_3O_4/CNF/BN/PA under different conditions (0.8 A, 1.0 A, 1.2 A and 1.4 A).

showed distinct steps, indicating the release of thermal energy from the CPCMs.

The energy conversion performance of CPCMs is a key property of interest in practical applications. A xenon lamp light source was used to simulate sunlight for photothermal conversion, a constant-voltage power supply generated a magnetic field through an inductive coil for magnetothermal conversion, and the temperature change of the CPCMs was recorded using a thermocouple (Fig. 7a and b). As the xenon lamp light source was turned on, the temperature of the CPCMs increased. When the light source was turned off, the temperature decreased gradually. As shown in Fig. 7c, the performance of the CPCMs improved progressively with the addition of functional components. The incorporation of CNF improved the heat transfer pathways of the material, allowing it to reach higher temperatures in a shorter period of time. The highest temperature of mica-Fe_3O_4/CNF/BN/PA under the same light conditions reached 85.9 °C. The photothermal conversion efficiency (η) of the CPCMs was calculated using the equation $\eta = m \times \Delta H/(I \times S \times \Delta t)$, where m and ΔH are the mass of the sample and the enthalpy of phase change during melting, respectively; I and S are the light intensity and illuminated area, respectively; and Δt is the duration of the phase-change process.[34] Compared to mica/PA (66.33%), mica/BN/PA (58.17%), and mica/CNF/BN/PA (62.53%), the photothermal conversion efficiency of mica-Fe_3O_4/CNF/BN/PA reached 88.36%, indicating that the composite materials have great potential for improving solar energy utilization efficiency. In addition, when compared with previously reported CPCMs, such as RGRCM-6 (78.7%), PW-CNTS (60.0%), CNT-silica (82.0%),[35–37] mica-Fe_3O_4/CNF/BN/PA exhibited higher photothermal conversion performance, further highlighting its promising potential in the field of solar energy utilization.

To broaden the application range of CPCMs in different environments, the magnetothermal transition properties of the CPCMs were further investigated to ensure proper functionality even under lightless conditions, such as cloudy or rainy days. To simulate the melting and crystallization processes of the PCM under different magnetic field strengths, the current was varied while the voltage was kept constant, allowing observation of the heating and cooling behaviors of mica-Fe_3O_4/CNF/BN/PA. From the temperature–time curves (Fig. 7d), a similar trend to the photothermal conversion process could be observed. The magnetothermal conversion efficiency of the CPCMs increased

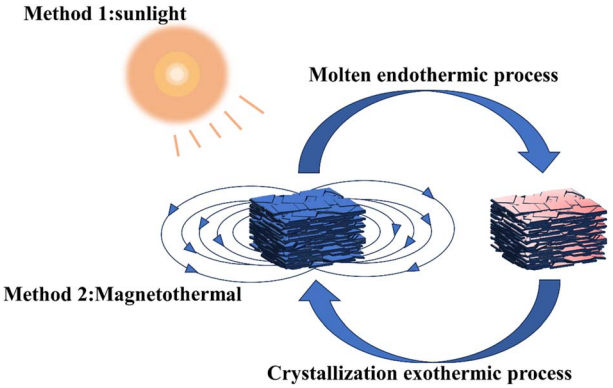

Fig. 8 Schematic of photothermal conversion and magnetothermal conversion.

progressively with increasing current. Accordingly, it took 112, 174, 245, and 277 s for mica-Fe_3O_4/CNF/BN/PA to complete the phase transition process under currents of 1.4 A, 1.2 A, 1.0 A and 0.8 A, respectively, with corresponding maximum temperatures reaching 86.1 °C, 82.9 °C, 63.6 °C, and 50.4 °C. The time required for phase transition directly reflected the magnetothermal conversion efficiency of the CPCMs. The above results indicate that mica-Fe_3O_4/CNF/BN/PA exhibits excellent magnetothermal conversion performance.

As shown in Fig. 8, the laminated structure of mica fixed the PCM on its surface and within its interstitial spaces. The addition of BN, metal oxide particles, and CNF improved the thermal conductivity and heat transfer pathways of the composite material. When light was irradiated onto the surface of mica, the CPCMs began to absorb light energy. The energy of photons was converted into thermal motion of PCM molecules, increasing their internal energy. As the temperature increased, the PCM underwent a phase change from solid to liquid. Once the phase change was complete, the additional absorbed thermal energy was stored in the PCM, completing the photothermal conversion process.

The surface-loaded Fe_3O_4 of layered mica caused the CPCM to exhibit magnetothermal transition properties. In the presence of an applied magnetic field, the magnetic moments or domains in the magnetic material underwent reorientation, transitioning from one ordered magnetic state to another. This process usually requires the rotation of magnetic moments or the movement of the walls of the magnetic domains, which consumes energy. The CPCMs absorbed magnetic energy, resulting in an increase in temperature. This heat absorption continued until an equilibrium state was reached. Afterward, the PCM underwent a phase change, completing the magnetothermal transition process.

4. Conclusions

In summary, dual-driven CPCMs were obtained by filling a PCM onto the laminated structure of mica using the vacuum impregnation method. FTIR, XRD, and XPS results confirmed that Fe_3O_4 was deposited on the surface of mica, and the preparation process did not change the chemical structure of the CPCMs. The introduction of BN and CNF improved the thermal conductivity of the CPCMs and formed heat transfer channels, enhancing the composite material's thermal performance and shape stability. Fe_3O_4 deposited on the surface of mica endowed the CPCMs with excellent dual-drive energy conversion performance. The mica-based CPCMs, with multiple types of energy conversion performance, have broad application prospects in multiple fields. The simple surface deposition of metal particles to modify the carrier provides valuable insights for the development of multifunctional energy conversion composites.

Data availability

All relevant data are included in the paper.

Conflicts of interest

The authors have reported no potential competing interests.

Acknowledgements

The authors gratefully acknowledge the support of the National Natural Science Foundation of China (NSFC, No. 21978074) and the Research Funding of Wuhan Polytechnic University (2024RZ044).

References

1 L. Yang, N. Zhang, Y. Yuan, X. Cao and B. Xiang, Thermal performance of stearic acid/carbon nanotube composite phase change materials for energy storage prepared by ball milling, *Int. J. Energy Res.*, 2018, **43**(12), 6327–6336, DOI: 10.1002/er.4352.

2 Y. Wu, X. Zhang, X. Xu, X. Lin and L. Liu, A review on the effect of external fields on solidification, melting and heat transfer enhancement of phase change materials, *J. Energy Storage*, 2020, **31**, 101567, DOI: 10.1016/j.est.2020.101567.

3 K. Pushpendra and K. Shailendra, Potential of macroencapsulated PCM for thermal energy storage in buildings: a comprehensive review, *Constr. Build. Mater.*, 2019, **225**, 723–744, DOI: 10.1016/j.conbuildmat.2019.07.221.

4 T. Qiu, J. Yang and X. Bai, Insight into the change in carbon structure and thermodynamics during anthracite transformation into graphite, *Int. J. Miner. Metall. Mater.*, 2020, **27**, 162, DOI: 10.1007/s12613-019-1859-9.

5 Y. Yu, Y. Zhou, Y. Zhang, Y. Zhang, X. Liu, X. Liang, J. Liu, S. Chen and W. Xiang, Novel $CsPbX_3$@mica composites with excellent optical properties for high efficiency and wide color gamut white light-emitting diode, *J. Lumin.*, 2021, **236**, 118129, DOI: 10.1016/j.jlumin.2021.118129.

6 J. Lv, J. Wang, J. Wang, T. Zhang, B. Yang, Z. Zhen, Y. Zheng and Y. Wang, Nanofibrous films embedded with phase change material: Flexible and photo- responsive dressings

for thermal compress therapy, *J. Energy Storage*, 2023, 106609, DOI: 10.1016/j.est.2023.106609.

7 G. Elisa and V. Vittorio, Thermal energy storage in district heating and cooling systems: a review, *Appl. Energy*, 2019, **252**, 113474, DOI: 10.1016/j.apenergy.2019.113474.

8 G. Li, Sensible heat thermal storage energy and exergy performance evaluations, *Renew. Sustainable Energy Rev.*, 2016, **53**, 897–923, DOI: 10.1016/j.rser.2015.09.006.

9 R. Bharathiraja, T. Ramkumar, M. Selvakumar and N. Radhika, Thermal characteristics enhancement of paraffin wax phase change material (PCM) for thermal storage applications, *Renew. Energy*, 2024, **222**, 119986, DOI: 10.1016/j.renene.2024.119986.

10 Y. Hu, M. Zhang, B. Quan, X. Li, X. Hu, H. Wu, X. Huang, X. Lu and J. Qu, Polyethylene glycol infiltrated biomass-derived porous carbon phase change composites for efficient thermal energy storage, *Adv. Compos. Hybrid Mater.*, 2024, **7**, 68, DOI: 10.1007/s42114-024-00880-z.

11 M. Zahir, S. Mohamed, R. Saidur and F. Al-Sulaiman, Supercooling of phasechange materials and the techniques used to mitigate the phenomenon, *Appl. Energy*, 2019, **240**, 793–817, DOI: 10.1016/j.apenergy.2019.02.045.

12 X. Deng, C. Li, X. Sun, C. Wang, B. Liu, Y. Li and H. Yang, Flame-retardant wood-based composite phase change materials based on PDMS/expanded graphite coating for efficient solar-to-thermal energy storage, *Appl. Energy*, 2023, **368**, 123454, DOI: 10.1016/j.apenergy.2024.123454.

13 A. Karaipekli and A. Sarı, Capric–myristic acid/vermiculite composite as form-stable phase change material for thermal energy storage, *Sol. Energy*, 2009, **83**, 323–332, DOI: 10.1016/j.solener.2008.08.012.

14 C. Li, B. Xie, J. Chen, Z. He, Z. Chen and Y. Long, Emerging mineral-coupled composite phase change materials for thermal energy storage, *Energy Convers. Manage.*, 2019, **183**, 633–644, DOI: 10.1016/j.enconman.2019.01.021.

15 Y. Zhang, S. Zheng, S. Zhu, J. Ma, Z. Sun and M. Farid, Evaluation of paraffin infiltrated in various porous silica matrices as shape-stabilized phase change materials for thermal energy storage, *Energy Convers. Manage.*, 2018, **171**, 361–370, DOI: 10.1016/j.enconman.2018.06.002.

16 C. Gayner, H. Kim, J. Kim and W. Kim, Spacer strategy for exceptionally low thermal conductivity and high zT in antimony-doped bulk silicon, *Mater. Today Energy*, 2019, **12**, 327–335, DOI: 10.1016/j.mtener.2019.03.001.

17 X. Chen, Z. Tang, P. Liu, H. Gao, Y. Chang and G. Wang, Smart utilization of multifunctional metal oxides in phase change materials, *Matter*, 2020, **3**, 708–741, DOI: 10.1016/j.matt.2020.05.016.

18 H. Ma and M. Xue, Recent advances in the photothermal applications of two-dimensional nanomaterials: photothermal therapy and beyond, *J. Mater. Chem. A*, 2021, **9**, 17569–17591, DOI: 10.1039/d1ta04134g.

19 Z. Tao, M. Yang, L. Wu, J. Yan, F. Yang, J. Lin, J. Wang and G. Wang, Phase change material based on polypyrrole/Fe_3O_4 functionalized hollow kapok fiber aerogel matrix for solar/magnetic-thermal energy conversion and storage, *Chem. Eng. J.*, 2021, **423**, 130180, DOI: 10.1016/j.cej.2021.130180.

20 G. Xin, H. Sun, S. Scott, T. Yao, F. Lu, D. Shao, T. Hu, G. Wang, G. Ran and J. Lian, Advanced phase change composite by thermally annealed defect-free graphene for thermal energy storage, *ACS Appl. Mater. Interfaces*, 2014, **6**, 15262–15271, DOI: 10.1021/am503619a.

21 Z. Tang, P. Cheng, P. Liu, Y. Gao, X. Chen and G. Wang, Tightened 1D/3D carbon heterostructure infiltrating phase change materials for solar-thermoelectric energy harvesting: faster and better, *Carbon Energy*, 2023, **5**, e281, DOI: 10.1002/cey2.281.

22 C. Feng, F. Wei, K. Sun, Y. Wang, H. Lan, H. Shang, F. Ding, L. Bai, J. Yang and W. Yang, Emerging flexible thermally conductive films: mechanism, fabrication, application, *Nano-Micro Lett.*, 2022, **14**(1), 127, DOI: 10.1007/s40820-022-00868-8.

23 J. Yang, X. Shen, W. Yang and J. Kim, Templating strategies for 3D-structured thermally conductive composites: recent advances and thermal energy applications, *Prog. Mater. Sci.*, 2023, **133**, 101054, DOI: 10.1016/j.pmatsci.2022.101054.

24 Y. Guo, K. Ruan and J. Gu, Controllable thermal conductivity in composites by constructing thermal conduction networks, *Mater. Today Phys.*, 2021, **20**, 100449, DOI: 10.1016/j.mtphys.2021.100449.

25 X. Yang, S. Fan, Y. Li, Y. Guo, Y. Li, K. Ruan, S. Zhang, J. Zhang, J. Kong and J. Gu, Synchronously improved electromagnetic interference shielding and thermal conductivity for epoxy nanocomposites by constructing 3D copper nanowires/thermally annealed graphene aerogel framework, *Compos. Part A Appl. Sci. Manuf.*, 2020, **128**, 105670, DOI: 10.1016/j.compositesa.2019.105670.

26 C. Pan, X. Li, G. Fan, Y. Long, Q. Chen, H. Yang and F. Wu, Modified mica-supported phase change materials for efficient solar thermal conversion and thermal energy management, *Appl. Therm. Eng.*, 2024, **236**, 121701, DOI: 10.1016/j.applthermaleng.2023.121701.

27 D. Hu, L. Han, W. Zhou, P. Li, Y. Huang, Z. Yang and X. Jia, Flexible phase change composite based on loading paraffin into cross-linked CNT/SS network for thermal management and thermal storage, *Chem. Eng. J.*, 2022, **437**, 135056, DOI: 10.1016/j.cej.2022.135056.

28 B. Lu, Y. Zhang, J. Zhang, J. Zhu, H. Zhao and Z. Wang, Preparation optimization and thermal characterization of paraffin/nano-Fe_3O_4 composite phase change material for solar thermal energy storage, *J. Energy Storage*, 2021, **46**, 103–928, DOI: 10.1016/j.est.2021.103928.

29 B. Ilíc, V. Radonjanin, M. Malešev, M. Zdujíc and A. Mitrovíc, Effects of mechanical and thermal activation on pozzolanic activity of kaolin containing mica, *Appl. Clay Sci.*, 2016, **123**, 173–181, DOI: 10.1016/j.clay.2016.01.029.

30 Z. Ma, Z. Deng, X. Zhou, L. Li, C. Jiao, H. Ma, Z. Yu and H. Zhang, Multifunctional and magnetic MXene composite aerogels for electromagnetic interference shielding with low reflectivity, *Carbon*, 2023, **213**, 118260, DOI: 10.1016/j.carbon.2023.118260.

31 Z. Liu, X. Fan, M. Han, H. Li, J. Zhang, Q. Zhu and J. Gu, Branched fluorine/adamantane interfacial compatibilizer for PBO fibers/cyanate ester wave-transparent laminated composites, *Chin. J. Chem.*, 2023, **40**, 939–950, DOI: **10.1002/cjoc.202200749**.

32 L. Tang, J. Yang, R. Bao, Z. Liu, B. Xie, M. Yang and W. Yang, Polyethylene glycol/graphene oxide aerogel shape-stabilized phase change materials for photo-to-thermal energy conversion and storage *via* tuning the oxidation degree of graphene oxide, *Energy Convers. Manage.*, 2017, **146**, 253–264, DOI: **10.1016/j.enconman.2017.05.037**.

33 L. Lv, Y. Wang, H. Ai, T. Chen, X. Zhang and S. Song, 3D graphene/silver nanowire aerogel encapsulated phase change material with significantly enhanced thermal conductivity and excellent solar-thermal energy conversion capacity, *J. Mater. Chem. A*, 2022, **10**, 7773–7784, DOI: **10.1039/d1ta10037h**.

34 W. Wang, B. Tang, B. Ju, Z. Gao, J. Xiu and S. Zhang, Fe_3O_4-functionalized graphene nanosheet embedded phase change material composites: efficient magnetic- and sunlight-driven energy conversion and storage, *J. Mater. Chem. A*, 2017, **5**, 958–968, DOI: **10.1039/c6ta07144a**.

35 Y. Zhou, X. Liu, D. Sheng, C. Lin, F. Ji and L. Dong, Polyurethane-based solid–solid phase change materials with *in situ* reduced graphene oxide for light-thermal energy conversion and storage, *Chem. Eng. J.*, 2018, **338**, 117–125, DOI: **10.1016/j.cej.2018.01.021**.

36 L. Chen, R. Zou, W. Xia, Z. Liu, Y. Shang and J. Zhu, Electro- and photodriven phase change composites based on wax-infiltrated carbon nanotube sponges, *ACS Nano*, 2012, **6**(12), 10884–10892, DOI: **10.1021/nn304310n**.

37 Y. Wang, L. Zhang and P. Wang, Self-floating carbon nanotube membrane on macroporous silica substrate for highly efficient solar-driven interfacial water evaporation, *ACS Sustainable Chem. Eng.*, 2015, **4**(3), 1223–1230, DOI: **10.1021/acssuschemeng.5b01274**.